J. Fluid Mech. (1986), *vol.* 166, *pp.* 173–187
Printed in Great Britain

Convection in a rotating cylindrical annulus: thermal Rossby waves

By F. H. BUSSE AND A. C. OR

Department of Earth and Space Sciences and Institute of Geophysics and Planetary Physics, University of California, Los Angeles, USA.

(Received 5 June 1985 and in revised form 25 November 1985)

The nonlinear equations describing convection in the form of thermal Rossby waves in a rotating annulus are solved both by an analytical perturbation theory and by a numerical method. It is shown that even in the absence of curvature of the surfaces bounding the fluid annulus in the axial direction a mean flow is generated by Reynolds stresses. The good agreement between analytical expressions and numerical results indicates that the former are valid over a larger domain of the parameter space than may be expected on the basis of the analysis of convection rolls in a non-rotating layer. This is caused in part by the reduced release of potential energy accompanying the reduced convective heat transport owing to the drift of the convection columns. The effect of curvature causes the replacement of the basic mode of convection by a different mode characterized by a double roll structure. The associated zonal mean flow is typically stronger than in the case without curvature.

1. Introduction

Convection driven by radial buoyancy in a rotating cylindrical annulus with conical end surfaces has long been recognized as a basic model for motions in stellar and planetary interiors. For a recent review see Busse (1982). But the problem is of more general interest to fluid dynamicists because of the time dependence of the convection columns and because of the generation of mean zonal flows by the fluctuating motions. Laboratory investigations of these phenomena are feasible since the centrifugal force can provide the appropriate buoyancy if the annular fluid region is heated from the outside and cooled from within (Busse & Carrigan 1974; Busse & Hood 1982; Azouni, Bolton & Busse 1986). The onset of convection, its time dependence, and the generation of zonal flows have been investigated in these laboratory studies.

The theory of the convection columns or thermal Rossby waves as they are sometimes called has been restricted so far to perturbation expansions of the solution up to the second order in the amplitude of convection. In this paper extensions of the previous analysis are described. The perturbation analysis is carried to higher order with the result that mean flows are found even in the case of end surfaces without curvature. The extent of the validity of the analytical perturbation expressions can be tested by a numerical integration of the basic equations. A Galerkin technique is introduced for this purpose and the dependent variables are expanded in terms of complete systems of functions. The nonlinear algebraic equations for the coefficients are then solved by a Newton–Raphson method. The numerical results match those of the truncated perturbation expansion over a remarkably wide interval. A stability analysis can be added in the numerical scheme in order to determine the domains

of stability of the steadily drifting convection columns. These results and the properties of the solutions bifurcating at the stability boundary will be discussed in a second paper (Or & Busse 1986) which will be referred to as II.

The paper starts with the formulation of the mathematical problem in §2. The perturbation analysis is described in §3 for the case without curvature. The corresponding numerical results are presented in §4. The analysis of the effect of curvature follows in §5. The paper closes with a discussion of mean zonal flows generated by convection and potential applications to the dynamics of planetary atmospheres.

2. Mathematical formulation

We consider a fluid-filled cylindrical annulus which is rotating about its axis of symmetry with the angular velocity Ω as shown in figure 1. The inner and the outer cylindrical walls are kept at the constant temperatures T_1 and T_2, respectively. Using the distance D between the walls as lengthscale, D^2/ν as timescale, where ν is the kinematic viscosity, and $P(T_2-T_1)$ as scale for the temperature, the Navier–Stokes equations of motion and the heat equation for the deviation θ from the state of pure conduction can be written in the following form

$$\frac{\partial}{\partial t}\boldsymbol{v}+\boldsymbol{v}\cdot\boldsymbol{\nabla}\boldsymbol{v}+2E^{-1}\boldsymbol{k}\times\boldsymbol{v}=-\boldsymbol{\nabla}\pi-R\theta\boldsymbol{i}+\nabla^2\boldsymbol{v}, \tag{2.1a}$$

$$\boldsymbol{\nabla}\cdot\boldsymbol{v}=0, \tag{2.1b}$$

$$\left(\frac{\partial}{\partial t}\theta+\boldsymbol{v}\cdot\boldsymbol{\nabla}\theta\right)P=-\boldsymbol{i}\cdot\boldsymbol{v}+\nabla^2\theta. \tag{2.1c}$$

The unit vectors $\boldsymbol{i}$ and $\boldsymbol{k}$ point in the radial and axial directions, and the dimensionless parameters of the problem are defined by

$$\text{Prandtl number:}\quad P\equiv\nu/\kappa,$$

$$\text{Rayleigh number:}\quad R\equiv\gamma D^3\Omega^2 r_0(T_2-T_1)/\nu\kappa,$$

$$\text{Ekman number:}\quad E\equiv\nu/D^2\Omega,$$

where κ, γ and r_0 denote the thermal diffusivity, the coefficient of thermal expansion, and the mean radius, respectively. We have neglected in equations (2.1) the variation of the centrifugal force and of the temperature gradient of the basic conductive state, since we shall introduce the small gap approximation, $D/r_0 \ll 1$. In this case a Cartesian system of coordinates can be introduced with the x- and z-coordinates in the directions of $\boldsymbol{i}$ and $\boldsymbol{k}$ and the y-coordinate in the azimuthal direction. We have also neglected the effect of gravity. This can be justified in laboratory applications of the theory if the axis of rotation is vertical and if the centrifugal force is of the same order as, or larger than, gravity (Busse 1970).

Among the boundary conditions the vanishing of the normal velocity component at the end surface is the most important one. Assuming symmetry with respect to the equatorial plane of the annulus and introducing the ratio l between axial length L and thickness D of the annulus we write this boundary condition in the form

$$\boldsymbol{v}\cdot[\boldsymbol{k}+i\eta_0(1+\epsilon f(x))]=0 \quad \text{at } z=\pm\tfrac{1}{2}l, \tag{2.2}$$

where η_0 is the average tangent of the angle between the conical end surfaces and the equatorial plane. For finite values ϵ, the end surfaces exhibit curvature in the

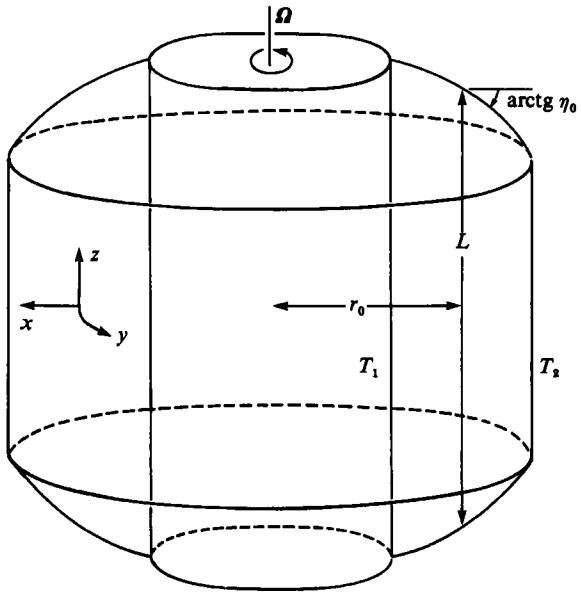

FIGURE 1. Geometrical configuration of the rotating fluid annulus.

radial direction, the dependence of which on x is described by the function $f(x)$. We shall assume that $f(x)$ is an increasing function of x with $f(-x) = -f(x)$. Assuming a positive η_0 we speak of the convex case for positive ϵ; the concave case corresponds to negative ϵ.

At the cylindrical walls we require stress-free, isothermal boundaries,

$$\boldsymbol{v}\cdot\boldsymbol{i} = \frac{\partial^2}{\partial x^2}\boldsymbol{v}\cdot\boldsymbol{i} = \theta = 0 \quad \text{at } x = \pm\tfrac{1}{2}. \tag{2.3}$$

Since the azimuthal wavelength of convection columns is typically small compared to the radial width, the difference between no-slip and stress-free conditions affects only a small region near the walls. An asymptotic theory can be developed for the limit of small E to take into account this difference; but such a boundary-layer analysis will not be attempted here. The main advantage of the boundary condition (2.3) is the possibility of a periodic continuation of the annular layer. An arrangement of stacked annular layers has been introduced in a model of the dynamics of Jupiter's atmosphere (Busse 1983*a*) and has been one of the motivations for the present analysis.

Additional conditions at $z = \pm\frac{1}{2}l$ are irrelevant in the following analysis. In particular Ekman layers formed at the end surfaces are unimportant as long as $\eta \cdot P \gg E^{\frac{1}{2}}$ holds according to Busse (1970). Since we are interested in the limit of small E which is relevant to laboratory experiments as well as to planetary applications, this inequality can be satisfied easily even if we require

$$\eta_0 \ll 1, \tag{2.4}$$

as we shall do in the following for reasons of mathematical convenience. For the analysis of the paper, insulating end surfaces provide the natural boundary condition for θ,

$$\frac{\partial}{\partial z}\theta = 0 \quad \text{at } z = \pm\tfrac{1}{2}l. \tag{2.5}$$

The limit (2.4) permits the assumption of nearly geostrophic solutions of (2.1),

$$\boldsymbol{v} = \boldsymbol{\nabla} \times \boldsymbol{k}\psi(x, y, t) + \check{\boldsymbol{v}}, \tag{2.6}$$

where $\check{\boldsymbol{v}}$ is a small perturbation of the order η_0. By taking the z-component of the curl of (2.1a), averaging it over z, and using the boundary condition (2.2) we obtain

$$\frac{\partial}{\partial t} \Delta_2 \psi + \bar{\boldsymbol{v}} \cdot \boldsymbol{\nabla} \Delta_2 \psi - 2\eta_0 [1 + \epsilon f(x)] (2E^{-1} - \Delta_2 \psi) \boldsymbol{i} \cdot \boldsymbol{v}|_{z=\frac{1}{2}l} l^{-1} = R \frac{\partial}{\partial y} \bar{\theta} + \nabla^2 \Delta_2 \psi, \tag{2.7}$$

where the bar indicates the average over z and the operator Δ_2 is defined by

$$\Delta_2 \equiv \frac{\partial^2}{\partial x^2} + \frac{\partial^2}{\partial y^2}.$$

We have used the definition

$$\Delta_2 \psi \equiv -\boldsymbol{k} \cdot \overline{\boldsymbol{\nabla} \times \boldsymbol{v}},$$

and have neglected the difference $\bar{\boldsymbol{v}} \cdot \boldsymbol{\nabla} \Delta_2 \psi - \overline{\boldsymbol{v} \cdot \boldsymbol{\nabla} \boldsymbol{k} \cdot \boldsymbol{\nabla} \times \boldsymbol{v}}$. To first order in η_0 we can replace $\boldsymbol{v}$ in (2.7) by the first term expression (2.6) and neglect the term $\Delta_2 \psi \boldsymbol{i} \cdot \boldsymbol{v}|_{z=\frac{1}{2}l}$ in comparison with the three nonlinear terms of the equation. We thus obtain

$$\left(\frac{\partial}{\partial t} + \frac{\partial}{\partial y}\psi \frac{\partial}{\partial x} - \frac{\partial}{\partial x}\psi \frac{\partial}{\partial y}\right) \Delta_2 \psi - \eta^* [1 + \epsilon f(x)] \frac{\partial}{\partial y} \psi - \Delta_2^2 \psi + R \frac{\partial}{\partial y} \theta = 0, \tag{2.8a}$$

where η^* is defined by

$$\eta^* \equiv 4\eta_0 / lE.$$

In accordance with the assumption of small η_0 the difference between θ and $\bar{\theta}$ can be neglected and the heat equation (2.1c) can be written

$$P\left(\frac{\partial}{\partial t} + \frac{\partial}{\partial y}\psi \frac{\partial}{\partial x} - \frac{\partial}{\partial x}\psi \frac{\partial}{\partial y}\right) \theta + \frac{\partial}{\partial y} \psi - \Delta_2 \theta = 0. \tag{2.8b}$$

Before solving the nonlinear problem posed by equations (2.8) we consider the linear limit. It is well known that solutions of the form

$$\psi_0 = \sin \pi(x + \tfrac{1}{2}) \sin(\alpha y + \omega t), \tag{2.9}$$

$$\theta_0 = -\alpha \sin \pi(x + \tfrac{1}{2}) \frac{P\omega_0 \sin(\alpha y + \omega t) + (\pi^2 + \alpha^2) \cos(\alpha y + \omega t)}{P^2 \omega_0^2 + (\pi^2 + \alpha^2)^2},$$

satisfy equations (2.8) and the boundary conditions (2.3) for $\epsilon = 0$ if the expressions

$$\omega = \omega_0 = -\frac{\eta^* \alpha}{(1+P)(\pi^2 + \alpha^2)}, \quad R_0 = (\pi^2 + \alpha^2)^3 \alpha^{-2} + \left(\frac{\eta^* P}{1+P}\right)^2 (\pi^2 + \alpha^2)^{-1}, \tag{2.10}$$

are chosen for the frequency and for the Rayleigh number, respectively. In the limit of large η^*, the value of α minimizing R_0 is given by

$$\alpha_c = \left(\frac{\eta^* P}{2^{\frac{1}{2}}(1+P)}\right)^{\frac{1}{3}}, \tag{2.11a}$$

and the minimum R_c of R_0 can be expressed in the form

$$R_c = 3\left[\frac{\eta^* P}{2^{\frac{1}{2}}(1+P)}\right]^{\frac{4}{3}}. \tag{2.11b}$$

In the next section the solution (2.9) will be extended into the nonlinear regime.

3. Perturbation analysis

By introducing the amplitude A of convection as a small parameter we can solve (2.8) in terms of an expansion in powers of A,

$$\left.\begin{aligned} \psi &= A(\psi_0 + A\psi_1 + A^2\psi_2 + \ldots), \\ \theta &= A(\theta_0 + A\theta_1 + A^2\theta_2 + \ldots), \\ R &= R_0 + AR_1 + A^2R_2 + \ldots, \\ \omega &= \omega_0 + A\omega_1 + A^2\omega_2 + \ldots. \end{aligned}\right\} \tag{3.1}$$

Restricting the attention to the case of vanishing curvature $\epsilon = 0$, and starting with the solution (2.9), (2.10) in the lowest order, we obtain in the order A^2 of (2.8),

$$\left(\frac{\omega_0}{\alpha}\frac{\partial}{\partial y} - \Delta_2\right)\Delta_2\psi_1 + R_0\frac{\partial}{\partial y}\theta_1 - \eta^*\frac{\partial}{\partial y}\psi_1 = \left(-\frac{\partial}{\partial y}\psi_0\frac{\partial}{\partial x} + \frac{\partial}{\partial x}\psi_0\frac{\partial}{\partial y}\right)\Delta_2\psi_0, \tag{3.2a}$$

$$\left(P\frac{\omega_0}{\alpha}\frac{\partial}{\partial y} - \Delta_2\right)\theta_1 + \frac{\partial}{\partial y}\psi_1 = P\left(-\frac{\partial}{\partial y}\psi_0\frac{\partial}{\partial x} + \frac{\partial}{\partial x}\psi_0\frac{\partial}{\partial y}\right)\theta_0. \tag{3.2b}$$

Since ψ and θ depend on y and t only through the combination $\alpha y + \omega t$ because of the wave character of the solution, we have replaced the time derivative by a y-derivative.

In writing (3.2) we have also anticipated that the solvability conditions require $R_1 = \omega_1 = 0$ because of the antisymmetry with respect to x of the inhomogeneous terms. Since the right-hand side of (3.2a) vanishes and the right-hand side of (3.2b) is independent of y, the solution of equations (3.2) assumes the form

$$\psi_1 = 0, \quad \theta_1 = B_1 \sin 2\pi(x + \tfrac{1}{2}), \tag{3.3}$$

with

$$B_1 \equiv P\alpha^2(\pi^2 + \alpha^2)\,[8\pi\omega_0^2 P^2 + 8\pi(\pi^2 + \alpha^2)^2]^{-1}.$$

As normalization condition we have imposed

$$\langle \psi_n \sin \pi(x + \tfrac{1}{2}) \exp\{\mathrm{i}\alpha y + \mathrm{i}\omega t\}\rangle = \tfrac{1}{4}\delta_{n0} \tag{3.4}$$

in order to eliminate phase shifts of the basic solution (2.9) introduced by higher-order terms. The angular brackets indicate the average over x- and y-coordinates. In the order A^3 of the problem, (2.8) assume the form

$$\left(\frac{\omega_0}{\alpha}\frac{\partial}{\partial y} - \Delta_2\right)\Delta_2\psi_2 + R_0\frac{\partial}{\partial y}\theta_2 - \eta^*\frac{\partial}{\partial y}\psi_2 = -R_2\frac{\partial}{\partial y}\theta_0 - \omega_2\alpha^{-1}\frac{\partial}{\partial y}\Delta_2\psi_0, \tag{3.5a}$$

$$\left(P\frac{\omega_0}{\alpha}\frac{\partial}{\partial y} - \Delta_2\right)\theta_2 + \frac{\partial}{\partial y}\psi_2 = -P\frac{\partial}{\partial y}\psi_0\frac{\partial}{\partial x}\theta_1 - \omega_2 P\alpha^{-1}\frac{\partial}{\partial y}\theta_0. \tag{3.5b}$$

To apply solvability conditions we must introduce the general solution

$$\psi^* = \sin \pi(x + \tfrac{1}{2}) \exp\{\mathrm{i}\alpha y + \mathrm{i}\omega t\}, \quad \theta^* = \mathrm{i}\alpha\psi^*[\pi^2 + \alpha^2 - \mathrm{i}P\omega_0]^{-1}, \tag{3.6}$$

of the adjoint linear homogeneous problem.

By multiplying (3.5a) by ψ^* and (3.5b) by $R_0\theta^*$, adding the equations and averaging them over the fluid layer we obtain a complex linear equation whose real and imaginary parts determine R_2 and ω_2 with the result

$$\omega_2 = 0, \quad R_2 = R_0 P\pi B_1. \tag{3.7}$$

The solution of equations (3.5), satisfying conditions (2.3) and (3.4), is given by

$$\psi_2 = R_0\,\alpha^2(\mathring{c}_2 \sin(\alpha y+\omega t)+\hat{c}_2\cos(\alpha y+\omega t))\sin 3\pi(x+\tfrac{1}{2}), \tag{3.8a}$$

$$\theta_2 = \alpha[((a_2^2\omega_0+\alpha\eta^*)\mathring{c}_2+a_2^4\hat{c}_2)\sin(\alpha y+\omega t)-(a_2^4\mathring{c}_2-(\omega_0 a_2^2+\alpha\eta^*)\hat{c}_2)\cos(\alpha y+\omega t)] \times\sin 3\pi(x+\tfrac{1}{2})-R_2\,\theta_0/R_0, \tag{3.8b}$$

where the definitions

$$\hat{c}_2 \equiv PB_1\,\pi[(1+P)\,\omega_0\,a_2^4+a_2^2\,\eta^*\alpha]\,E_2, \quad \mathring{c}_2 \equiv PB_1\,\pi[R_0\,\alpha^2-a_2^6+P\omega_0(a_2^2\,\omega_0+\eta^*\alpha)]\,E_2,$$

$$a_2^2 \equiv 9\pi^2+\alpha^2, \quad E_2 \equiv \{[R_0\,\alpha^2+P\omega_0(a_2^2\,\omega_0+\eta^*\alpha)-a_2^6]^2+[(1+P)\,\omega_0\,a_2^4+a_2^2\,\eta^*\alpha]^2\}^{-1},$$

have been used.

A novel result is obtained in the next higher order of the equations. For reasons of symmetry ω_3 and R_3 must vanish. But the solution for ψ_3 contains a mean component independent of y and t. By taking the y-average over the original equation of motion, the equation for the mean zonal flow $V_3 \equiv -\partial\overline{\psi}_3/\partial x$ can be written in the form

$$\frac{\partial^2}{\partial x^2}V_3 = -\frac{\partial}{\partial x}\overline{\left(\frac{\partial}{\partial x}\psi_2\frac{\partial}{\partial y}\psi_0+\frac{\partial}{\partial x}\psi_0\frac{\partial}{\partial y}\psi_2\right)}, \tag{3.9}$$

were the y-average has been indicated by a bar. (Since the z-dependence is no longer part of the problem, this bar should not be mistaken for the z-average used in §2.) Integration of (3.9) yields

$$V_3 = \tfrac{1}{8}\hat{c}_2\,\alpha^3 R_0[\cos 4\pi(x+\tfrac{1}{2})-4\cos 2\pi(x+\tfrac{1}{2})]. \tag{3.10}$$

This result demonstrates that a mean zonal flow with retrograde direction is generated in the interior of the annular layer for positive η^*. In contrast to the zonal flow generated by a finite curvature ϵ (Busse & Hood 1982), it is symmetric about the midplane of the layer. The constant of integration has been chosen such that $\langle V_3\rangle$ vanishes. In order to satisfy no-slip conditions required by rigid walls at $x = \pm\frac{1}{2}$, however, an appropriate constant can be added in expression (3.10).

Another mean quantity interest is $\bar{\theta}_3$ for which the equation

$$\frac{\partial^2}{\partial x^2}\bar{\theta}_3 = P\frac{\partial}{\partial x}\overline{\left[\theta_0\frac{\partial}{\partial y}\psi_2+\theta_2\frac{\partial}{\partial y}\psi_0\right]}, \tag{3.11}$$

holds. The solution of this equation satisfying the boundary condition (2.3) is given by

$$\bar{\theta}_3 = \{\alpha^4 R_0(\pi^2+\alpha^2)\,[P^2\omega_0^2+(\pi^2+\alpha^2)^2]^{-1}\,\mathring{c}_2+\alpha^2(a_2^4\,\mathring{c}_2-\omega_0\,a_2^2\,\hat{c}_2)\} \times\frac{(\sin 2\pi(x+\frac{1}{2})-\frac{1}{2}\sin 4\pi(x+\frac{1}{2}))}{4\pi}+\frac{R_2(\pi^2+\alpha^2)\,\alpha^2\sin 2\pi(x+\frac{1}{2})}{[P^2\omega_0^2+(\pi^2+\alpha^2)^2]\,4\pi R_0}. \tag{3.12}$$

A physical quantity of special interest is the convective heat transport. Usually it is described by the Nusselt number which is defined as the total heat transport across the layer in the presence of convection divided by the heat transport in the absence of convection,

$$Nu = 1+P\frac{\partial}{\partial x}\bar{\theta}\Big|_{x=\pm\frac{1}{2}}. \tag{3.13}$$

Taking into account only the lowest-order term we find

$$Nu-1 = \frac{2(R-R_0)}{R_0}+\ldots. \tag{3.14}$$

This expression is the same as in the case of a non-rotating layer heated from below. The absence of any dependence on P and η^* disappears, however, as higher-order terms are taken into account. Solution (3.12) indicates the complexity of higher-order terms that have been neglected in (3.14). The results of the numerical analysis discussed in the next section bear out this point.

4. Numerical analysis

The advantage of the perturbation analysis outlined in the preceding section lies in the derivation of expressions exhibiting an explicit dependence on the parameters η^*, P, α of the problem. But because of the necessity of truncating the perturbation series and because of its finite radius of convergence the results are useful only within a limited range of B. The numerical solution of (2.8) yields complementary results. While only selected parameter values can be used in general, relatively high values of B are accessible and by comparison with the perturbation theory the range of validity of the analytical expressions can be assessed.

In extension of earlier work on convection in a plane layer we use a Galerkin method for the numerical solution. By expanding the dependent variables ψ and θ in terms of functions satisfying the boundary conditions (2.2),

$$\left.\begin{aligned}\psi &= \sum_{l,\,n} \sin l\pi(x+\tfrac{1}{2})\{\hat{a}_{ln}\cos n\alpha(y-ct)+\check{a}_{ln}\sin n\alpha(y-ct)\},\\ \theta &= \sum_{l,\,n} \sin l\pi(x+\tfrac{1}{2})\{\hat{b}_{ln}\cos n\alpha(y-ct)+\check{b}_{ln}\sin n\alpha(y-ct)\},\end{aligned}\right\} \tag{4.1}$$

we obtain a system of nonlinear equations for the coefficients $\hat{a}_{km}$, $\check{a}_{km}$, $\hat{b}_{km}$ and $\check{b}_{km}$ after (2.8) have been multiplied by the expansion functions and averaged over the fluid layer. In order to solve the system of nonlinear algebraic equations we have to introduce a truncation procedure. We do so by neglecting all equations and all coefficients with subscripts l, n satisfying

$$l+n > N_{\mathrm{T}}, \tag{4.2}$$

where N_{T} is the truncation parameter. $N_{\mathrm{T}} = 6$ has been found to yield satisfactory results over nearly the entire range of Rayleigh numbers that has been investigated. Comparison with solutions for $N_{\mathrm{T}} = 8$ indicates that significant deviations appear only at the highest Rayleigh numbers studied. In fact, for much of the parameter domain shown in the following, solutions obtained with $N_{\mathrm{T}} = 4$ suffice.

In this section only results for vanishing curvature of the end surfaces, $\epsilon = 0$, will be discussed. In this case a subclass of solutions of the form (4.1) has the property that all coefficients with odd $l+n$ vanish. This subclass is of primary interest since it contains the solution corresponding to the minimum value of R for which the perturbation solution of §3 has been obtained. A comparison of numerical and analytical results is shown in figure 2. The straight lines indicate that the coefficients conform to the power-law dependence of the corresponding first terms of the perturbation series. Only when $(R-R_{\mathrm{c}})/R_{\mathrm{c}}$ reaches values of the order 1 do significant changes occur in the dependence of the coefficients on R. Most of these changes can be described as saturation effects in that the growth of the convection amplitude is weakened. This property is also evident in figure 3 where the Nusselt number is shown for different values of η^* and P. The most noticeable saturation of the Nusselt number occurs for $P = 1$. The phase shift between θ_0 and ψ_0 is 0 and $\frac{1}{2}\pi$ in the limits $P \to 0$ and $P \to \infty$, respectively, and thus the nonlinear interaction described by higher-order terms is strongest at some intermediate Prandtl number.

At higher values of η^* the remarkable phenomenon occurs that two solutions with

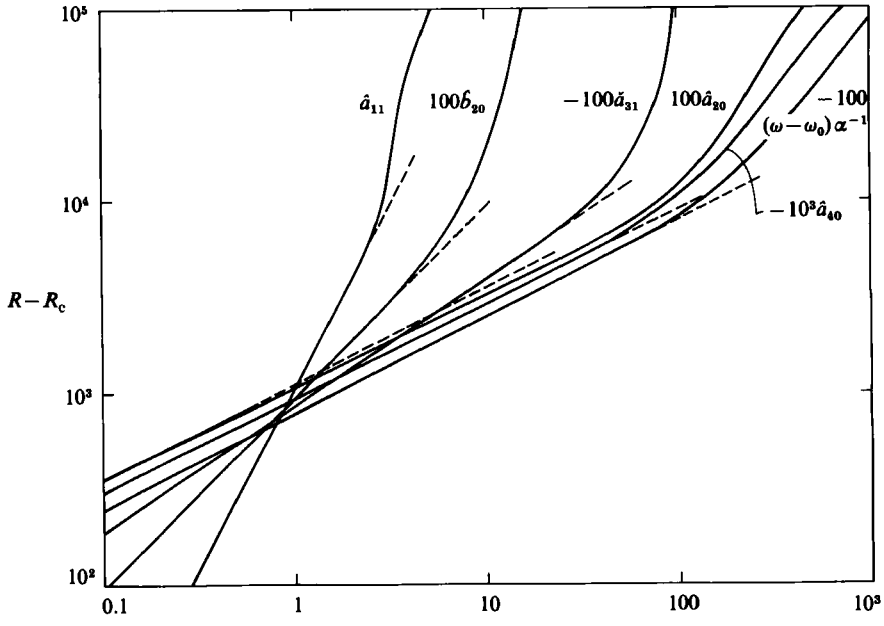

FIGURE 2. Comparison of numerical results with the analytical expressions (dashed lines) for $P = 1$, $\eta^* = 2800$, $\epsilon = 0$, $\alpha = \alpha_c = 9.4$. The critical value of R is $R_c = 30680$.

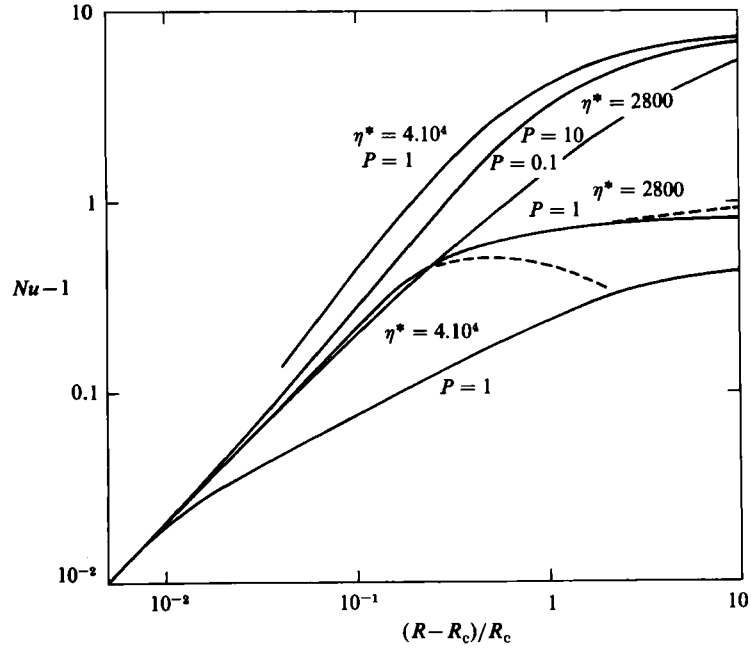

FIGURE 3.The Nusselt number Nu as a function of $(R-R_c)/R_c$ for various values of P and η^*. In the limit $R \to R_c$ the Nusselt number is independent of those two parameters according to (3.14). In the case $P = 1$, $\eta^* = 2800$ dashed curves obtained for lower values of the truncation parameter N_T are shown for comparison.

the same symmetry properties can be obtained at the same value of B. As shown in figure 3 for $\eta^* = 4 \cdot 10^4$ a lower branch bends away sharply, but smoothly, from the common line for low values of $R-R_c/R_c$, while a separate upper branch has been found at higher values of $R-R_c/R_c$. When it was attempted to continue the upper branch towards lower values that solution jumped to the lower branch. The nearly kink-like bend of the lower branch does not indicate a bifurcation, as has become evident from the stability analysis of the solutions. The lower branch remains stable with respect to disturbances of the same symmetry up to $R-R_c \approx 0.045\,R_c$, while the upper branch is always unstable with respect to these disturbances. A more complete discussion of the stability properties of various solutions will be given in II.

5. The effect of finite curvature

In the case of finite ϵ equations (2.8) do not permit simple solutions even in the linear limit of the problem. In order to study the dependence of the critical Rayleigh number on ϵ we thus shall employ a perturbation expansion in powers of ϵ,

$$\left.\begin{aligned} R &= R_0^{(n)} + \epsilon R_1^{(n)} + \epsilon^2 R_2^{(n)} + \ldots, \\ \omega &= \omega_0^{(n)} + \epsilon\omega_1^{(n)} + \epsilon^2\omega_2^{(n)} + \ldots, \\ \psi &= \psi_0^{(n)} + \epsilon\psi_1^{(n)} + \ldots, \end{aligned}\right\} \tag{5.1}$$

and use a particularly convenient form of the function $f(x)$,

$$f(x) = -\pi^{-1}\cos\pi(x+\tfrac{1}{2}). \tag{5.2}$$

We have introduced the superscript n because we start with the general solution

$$\left.\begin{aligned} \psi_0^{(n)} &= \sin n\pi(x+\tfrac{1}{2})\exp\{\mathrm{i}\alpha y + \mathrm{i}\omega t\}, \\ \omega_0^{(n)} &= -\alpha\eta^*(1+P)^{-1}(n^2\pi^2+\alpha^2)^{-1}, \\ R_0^{(n)} &= (n^2\pi^2+\alpha^2)^3\alpha^{-2} + \left(\frac{\eta^* P}{1+P}\right)^2 (n^2\pi^2+\alpha^2)^{-1} \end{aligned}\right\} \tag{5.3}$$

of the limit $\epsilon = 0$. In first order in ϵ we obtain

$$\left[\mathrm{i}\omega_0^{(n)} P + \alpha^2 - \frac{\partial^2}{\partial x^2}\right]\left\{\left(\mathrm{i}\omega_0^{(n)} + \alpha^2 - \frac{\partial^2}{\partial x^2}\right)\left(\alpha^2 - \frac{\partial^2}{\partial x^2}\right) + \mathrm{i}\alpha\eta^*\right\}\psi_1^{(n)} - \alpha^2 R_0^{(n)}\psi_1^{(n)}$$
$$= -\mathrm{i}\alpha\eta^*\left(\mathrm{i}\omega_0^{(n)} P + \alpha^2 - \frac{\partial^2}{\partial x^2}\right) f(x)\,\psi_0^{(n)}. \tag{5.4}$$

By combining (2.8a) and (2.8b) we have eliminated the variable θ. The terms involving $\omega_1^{(n)}$ and $R_1^{(n)}$ have been neglected because the solvability condition for (5.4) requires $\omega_1^{(n)} = R_1^{(n)} = 0$. The solution $\psi_1^{(n)}$satisfying the boundary conditions (2.3) is given by

$$\psi_1^{(n)} = \frac{\mathrm{i}\alpha\eta^*}{2\pi}\left(A_+ \sin(n+1)\pi(x+\tfrac{1}{2}) + A_- \sin(n-1)\pi(x+\tfrac{1}{2})\right), \tag{5.5}$$

where the definition

$$\begin{aligned} A_\pm \equiv\ & (\mathrm{i}\omega_0^{(n)} P + \alpha^2 + (n\pm 1)^2\pi^2)\,[\alpha^2(R_0^{(n\pm1)} - R_0^{(n)}) + \mathrm{i}(\omega_0^{(n\pm1)} - \omega_0^{(n)}) \\ & \times (1+P)\,(\alpha^2 + (n\pm1)^2\pi^2)^2 + (\omega_0^{(n)^2} - \omega_0^{(n\pm1)^2})\,(\alpha^2 + (n\pm1)^2\pi^2)\,P^2 \\ & - \omega_0^{(n)^2} P(1+P)\,(1\pm 2n)\,\pi^2]^{-1}, \end{aligned} \tag{5.6}$$

has been used.

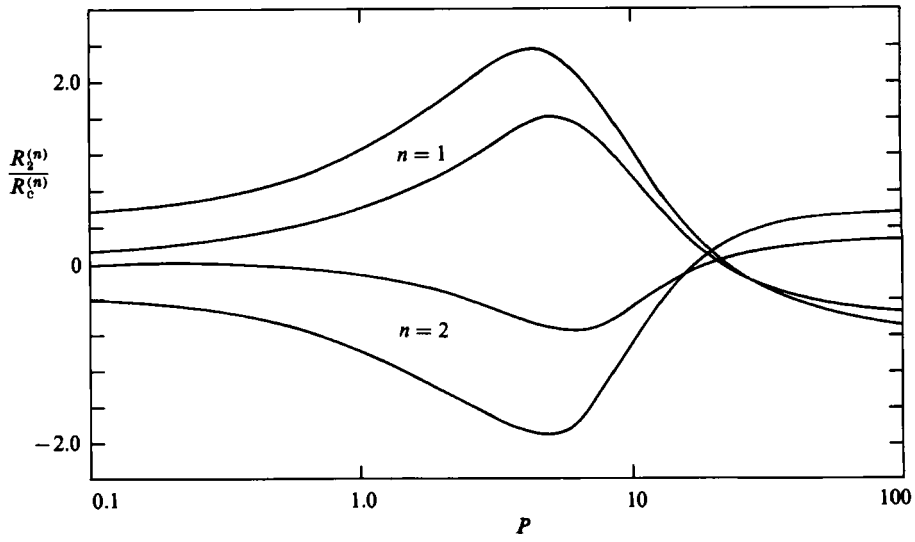

FIGURE 4. $R_2^{(n)}$ as a function of P for $n = 1, 2$. The outer curves show $10 \cdot R_2^{(n)}/R_c$ for $\eta^* = 2800$, the inner curves show $R_2^{(n)}/R_c$ for $\eta^* = 4 \cdot 10^4$.

The solvability condition in the order ϵ^2 is obtained by multiplying the equation for $\psi_2^{(n)}$ by $\psi_0^{(n)*}$ and averaging it over the fluid layer. Here the asterisk is used to indicate the complex conjugate. The result yields a complex equation for $\omega_2^{(n)}$ and $R_2^{(n)}$,

$$i\omega_2^{(n)} [(\alpha^2 + n^2\pi^2)^2 (1+P) + i\alpha\eta^* P(P-1)(P+1)^{-1}] - \alpha^2 R_2^{(n)} = \left(\frac{i\alpha\eta}{2\pi}\right)^2 (i\omega_0^{(n)} P + \alpha^2 + n^2\pi^2)[A_+ + A_-(1-\delta_{n1})]. \quad (5.7)$$

Figure 4 shows $R_2^{(n)}$ as a function of P for $n = 1, 2$ and two values of η^*. The interesting feature of figure 4 is the opposite sign of $R_2^{(1)}$ and $R_2^{(2)}$. For a significant range of intermediate Prandtl numbers the negative value of $R_2^{(2)}$ indicates that the $n = 2$ mode may replace the $n = 1$ mode as the critical disturbance for sufficiently high ϵ.

The numerical results obtained for finite ϵ confirm this expectation. The values $R_2^{(n)}$ for $n > 2$ exhibit a dependence on the Prandtl number similar to that of $R_2^{(2)}$ but the magnitudes of $R_2^{(n)}$ decrease with increasing n. Thus the mode $n = 2$ is the only mode capable of competing with the $n = 1$ mode at the critical Rayleigh number. The numerical results shown in figure 5 (a, b) correspond to a different function $f(x)$,

$$f(x) = x, \quad (5.8)$$

which is more useful for applications of the theory. Numerical results have also been obtained for the function (5.2) but they differ little from those shown in figure 4 and have not been plotted for this reason. At the points where the $n = 1$ mode and $n = 2$ mode do not only nearly agree with respect to the value R but with respect to the frequency ω as well, a switch-over phenomenon occurs, as is evident in the case $\epsilon = 0.75$ in figure 5 (a, b). The solution of the $n = 1$ type becomes a solution of the $n = 2$ type and vice versa. This is possible because the two solutions are indistinguishable at the point where both satisfy the equation for identical values of the parameters.

It must be expected that the highest amplitude of the preferred mode of convection occurs in the part of the annular region where the constraining effect of rotation is

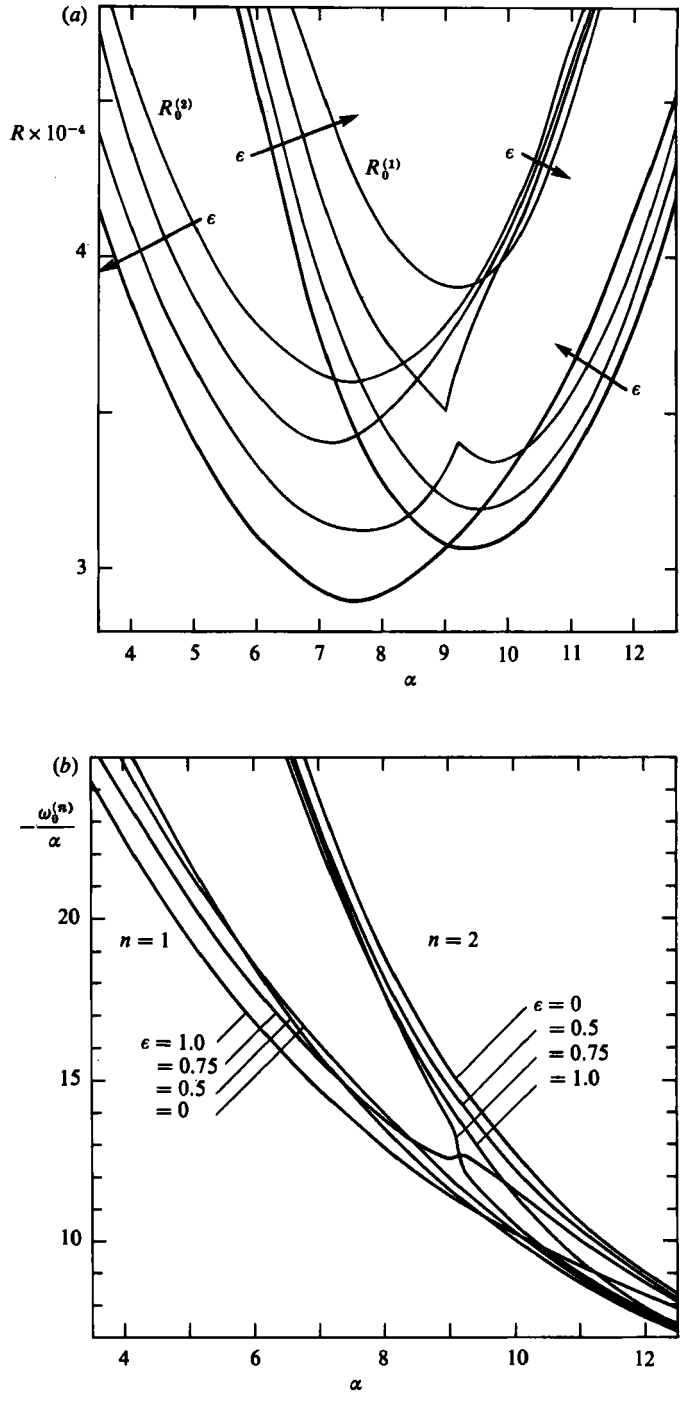

FIGURE 5. (*a*) The Rayleigh numbers of the linear problem, $R_0^{(1)}$ and $R_0^{(2)}$, as a function of the wavenumber α in the case $P = 1$, $\eta^* = 2800$. The four curves in each case correspond to $\epsilon = 0$, 0.5, 0.75 and 1.0. The arrows indicate the direction of increasing ϵ. (*b*) As (*a*) except that the driftrates $c^{(n)} = -\omega_0^{(n)}/\alpha$ are plotted as a function of α.

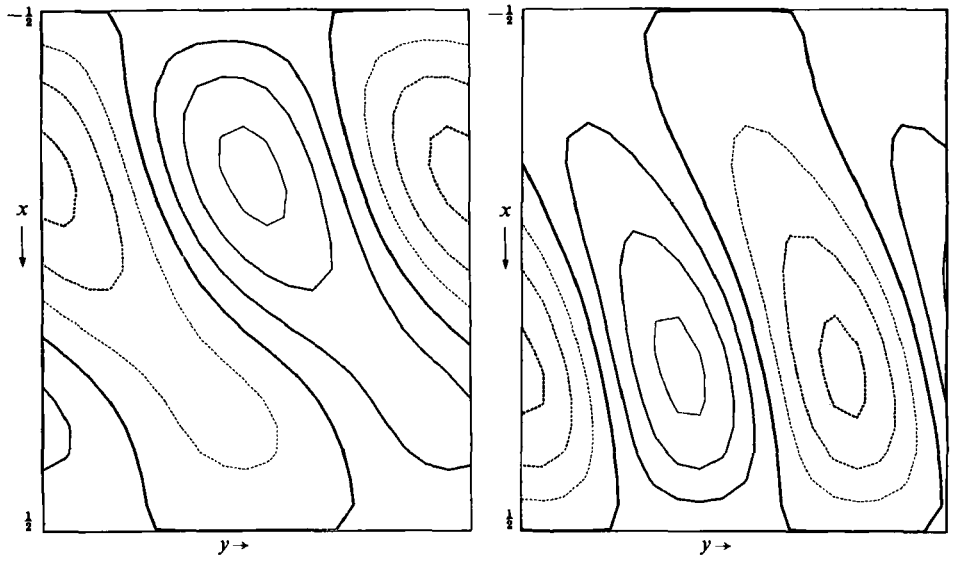

FIGURE 6. Streamlines $\psi^{(n)} = \text{const.}$ for $\eta^* = 2800$, $\epsilon = 1$, $P = 0.7$. The graph on the left side corresponds to $n = 2$, $R = 34510$, $\alpha = 6.8$, $c = 18.08$; the graph on the right side corresponds to $n = 1$, $\alpha = 8.7$, $R = 43660$. The dashed lines give negative value of $\psi^{(n)}$.

lowest, i.e. in the region of negative x when ϵ is positive. This property is borne out by the eigenfunctions of the modes $n = 1$ and $n = 2$ for $P \lesssim 1.5$ and $P \gtrsim 20$. In the region where $R_2^{(n)}$ is negative the respective mode exhibits a maximum of $|\psi^{(n)}|$ in the interval $-\frac{1}{2} < x < 0$, while the mode with positive $R_2^{(n)}$ exhibits a maximum amplitude in the outer part, $x > 0$, of the annular layer. However, in the intermediate range of Prandtl numbers, $1.5 \lesssim P \lesssim 20$, the mode $n = 2$ has a maximum amplitude for $x > 0$, even though the negative value of R_2 indicates a physical preference, at least for larger values of ϵ. The exact boundaries of the interval $1.5 \lesssim P \lesssim 20$ depend of course on η^*. The lower boundary $P = 1.5$ corresponds to the asymptotic value in the limit $\eta^* \rightarrow \infty$ which was analysed by Busse & Hood (1982).

A graph of the streamlines of modes $n = 1, 2$ is shown in figure 6 for the Prandtl number $P = 0.7$. The graphs are based on computations with the function (5.8) and with $\epsilon = 1$. The streamline patterns show the opposite location of the maxima of the two modes and the characteristic slanted structure which is found in all computations for positive ϵ. For negative ϵ the streamlines will be slanted in the other way.

6. Discussion

The slanted form of the convection columns shown in figure 6 indicates a strong momentum transport towards the outside for $\epsilon > 0$. This effect has been studied theoretically and experimentally by Busse & Hood (1982). The numerical method described in §4 permits a more detailed investigation of the mean flow generation process. Since the subclass of solutions of the form (4.1) with vanishing coefficients for odd $l+n$ no longer exists for finite ϵ, the boundary conditions for the mean flow part of the solutions become important. In order to make the nonlinear analysis comparable with the case $\epsilon = 0$ and with the analytical theory of Busse (1983*a*),

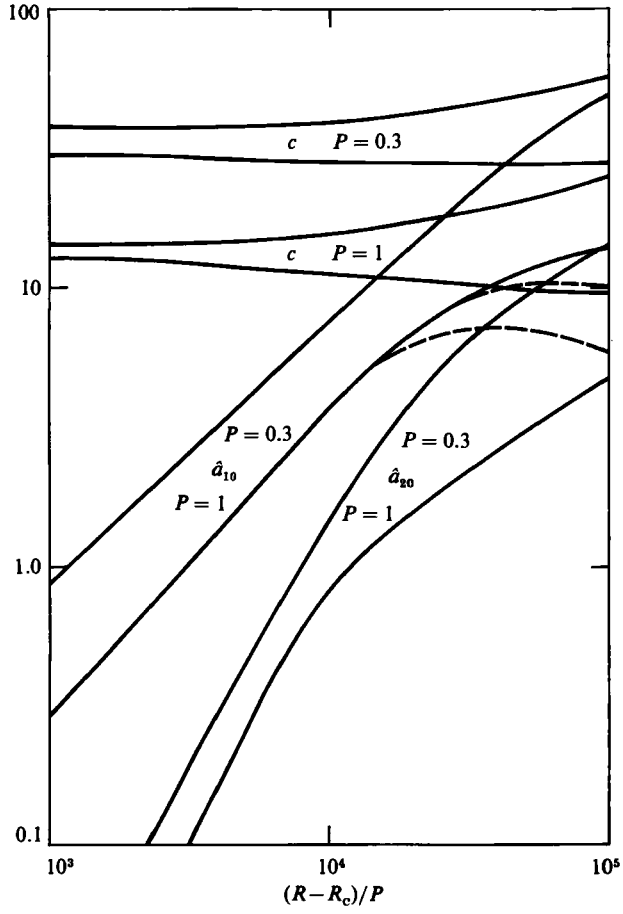

FIGURE 7. Comparison of solutions for $\epsilon = 0$ and $\epsilon = 1$ at two Prandtl numbers $P = 1$, $P = 0.3$, each. The mean flow properties are characterized by the coefficients $\hat{a}_{20}$ in the case $\epsilon = 0$ and $\hat{a}_{10}$ in the case $\epsilon = 1$. The phase velocity $c = -\omega/\alpha$ increases with $R-R_c$ for $\epsilon = 0$ (upper curve) and decreases for $\epsilon = 1$ (lower curve). The value of α chosen in each case is close to the respective critical value α_c. Dashed lines indicate solutions with $N_T = 4, 6$. The solid lines correspond to $N_T = 8$.

periodic boundary conditions have been imposed. These conditions require the replacement of the term $\hat{a}_{l0} \sin l\pi(x+\frac{1}{2})$ in (4.1) by

$$\hat{a}_{l0}(\sin l\pi(x+\tfrac{1}{2}) + (x^2-\tfrac{1}{4})\, l\pi), \tag{6.1}$$

whenever l is an odd integer. The mean flow obtained by this procedure is shown in figure 7. Since the coefficient $\hat{a}_{10}$ provides the dominant contribution, the other coefficients have not been plotted. Clearly, the asymmetric mean flow of the case $\epsilon = 1$ is always much larger than the symmetric flow found in the case $\epsilon = 0$. Both cases, $\epsilon = 0$ and $\epsilon = 1$, show a similar saturation of the mean zonal flow which becomes noticeable for large values of $R-R_c$.

In the computations of the finite amplitude solution for $\epsilon = 1$ the mode $n = 2$ of the linear analysis has been used as a starting point since this mode corresponds to the preferred solution for the Prandtl numbers $P = 0.3$ and $P = 1$. In this respect the present analysis differs from the perturbation analysis of Busse & Hood (1982) where only the mode $n = 1$ was considered. Since the tilt of the linear solutions with

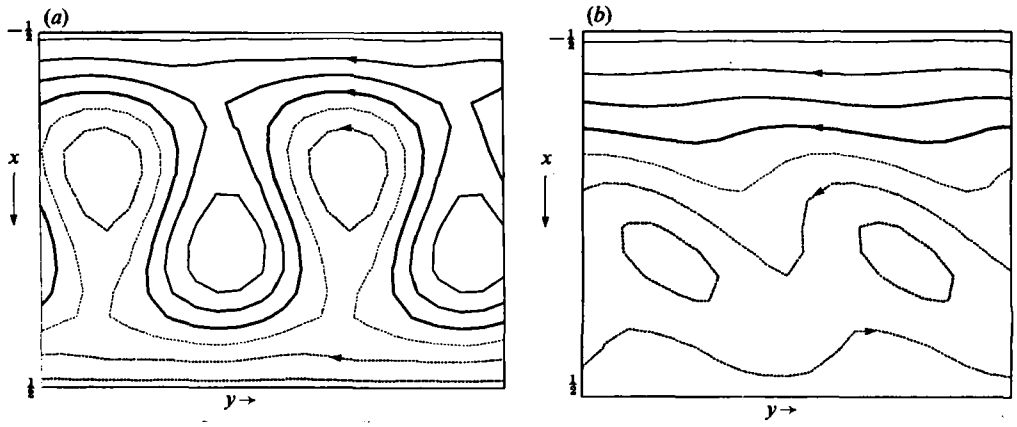

FIGURE 8. Streamline patterns of stationary convection flow as seen from the drifting frame of reference. Solid (broken) lines indicate positive (negative) values of the streamfunction. Example (*a*) corresponds to $\epsilon = 0$, $\eta^* = 2200$, $P = 1$, $R = 5 \times 10^5$, $\alpha = 9.0$; (*b*) corresponds to $\epsilon = 0.5$, $\eta^* = 2800$, $R = 1.2 \times 10^5$, $\alpha = 9.0$, $c = 10.3$ In (*a*) the mean shear is cyclonic (anticyclonic) for $x < 0$ ($x > 0$), while in (*b*) the mean shear is cyclonic throughout the layer.

respect to the x-axis is quite similar for both modes in the case $\epsilon = 1$, the mean zonal flow generated by the fluctuating convection columns does not differ much at finite amplitudes of the modes $n = 1$ and $n = 2$. The profile of the mean flow also does not change much as a function of the Prandtl number while its amplitude varies with P as indicated in figure 7. The latter feature agrees qualitatively with the perturbation solution of Busse & Hood (1982). Thus the general conclusions of that paper remain valid although they are based on a more restricted analysis.

In order to visualize solutions of the form (4.1), (6.1), it is convenient to plot lines of constant ψ with respect to the drifting frame of reference in which the solutions are steady and the lines of constant ψ can be interpreted as streamlines. Since the velocity c in the negative y-direction must be added in the frame of reference drifting with the velocity c in the positive y-direction, the streamline graph does not show closed streamlines for weak amplitudes of convection. Only when the amplitude of convection and the mean flow generated by it become sufficiently strong, do closed streamlines appear as shown for example in figure 8. Figure 8(*a*) reflects the symmetry of the problem with respect to the plane $x = 0$ in the case $\epsilon = 0$. Cyclonic and anticyclonic eddies are equally strong. Since the mean shear generated in the case $\epsilon > 0$ is predominantly cyclonic, only cyclonic close streamlines are visible in figure 8(*b*).

One of the main motivations for the present analysis has been the desire for a better understanding of the atmospheric dynamics of the major planets. While the mean zonal flows of Jupiter and Saturn can be interpreted quite well in terms of relatively simple models (Busse 1983*a*, *b*), the fluctuating motions appear to be much more complex. Although fairly regularly spaced eddies are seen in the *Voyager* pictures of Jupiter, the morphology of these motions varies strongly with latitude and exhibits little symmetry with respect to the equator. Most of the small-scale dynamic features, including the white ovals and the Red Spot, are probably confined to the upper stably stratified layer of the Jovian atmosphere. The most direct evidence for convection flow is likely to come from features connected with the deeper unstably stratified atmosphere.

A peculiar feature which exhibits dynamic properties of the convection columns

discussed in this paper are the plumes observed at the northern edge of the equatorial zone of Jupiter (Mitchell *et al.* 1979). The heads of those plumes appear to drift in the prograde direction relative to the surrounding medium. The plumes thus extend in the westward or retrograde direction. This particular latitude is characterized by a strong cyclonic shear and may represent a particular annular convection layer which is coaxial with the rotation axis of the planet.

While an association of the plume heads with cyclonic eddies has not yet been established, cyclonic eddies are seen at higher latitudes. For example, the dark spots called barges correspond to deeper layers of the atmosphere and thus could well be manifestations of convective activity in the Jovian interior. Obviously, the connection between the nonlinear solutions studied in this paper and the observations is tentative. But the investigation of the properties of the nonlinear thermal Rossby waves and of the secondary and tertiary solutions that bifurcate from them is likely to provide a basis for the improved understanding of the dynamical features observed on the major planets.

The research reported in this paper has been supported by the Atmospheric Sciences Section of the U.S. National Science Foundation.

REFERENCES

AZOUNI, A., BOLTON, E. W. & BUSSE, F. H. 1986 Experimental study of convection columns in a rotating cylindrical annulus. *Geophys. Astrophys. Fluid Dyn.* **34**, 301–317.

BUSSE, F. H. 1970 Thermal instabilities in rapidly rotating systems. *J. Fluid Mech.* **44**, 441–460.

BUSSE, F. H. 1982 Thermal convection in rotating systems. *Proc. 9th U.S. National Congress of Appl. Mech. ASME, New York, N.Y. 1982*, pp. 299–305.

BUSSE, F. H. 1983*a* A model of mean zonal flows in the major planets. *Geophys. Astrophys. Fluid Dyn.* **23**, 153–174.

BUSSE, F. H. 1983*b* Convection-driven zonal flows in the major planets. *PAGEOPH* **121**, 375–390.

BUSSE, F. H. & CARRIGAN, C. R. 1974 Convection induced by centrifugal buoyancy. *J. Fluid Mech.* **62**, 579–592.

BUSSE, F. H. & HOOD, L. L. 1982 Differential totation driven by convection in a rotating annulus. *Geophys. Astrophys. Fluid Dyn.* **21**, 59–74.

MITCHELL, J. L., TERRILE, R. J., SMITH, B. A., MULLER, J.-P., INGERSOLL, A. P., HUNT, G. E., COLLINS, S. A. & BEEBE, R. F. 1979 Jovian cloud structure and velocity fields. *Nature* **280**, 776–778.

OR, A. C., & BUSSE, F. H. 1986 Convection in a rotating cylindrical annulus. Part 2. Transitions to asymmetric and vacillating flow. Submitted to *J. Fluid Mech.*